DESIGN OF A GH2/GOX COMBUSTION CHAMBER FOR THE HOT PLUME INTERACTION EXPERIMENTS AT DLR COLOGNE

Dominik Saile[1], Daniel Kirchheck[1], Ali Gülhan[1], Chadi Serhan[2], and Volker Hannemann[2]

[1]*DLR, German Aerospace Center, Institute of Aerodynamics and Flow Technology, 51147 Cologne, Germany*
[2]*DLR, German Aerospace Center, Institute of Aerodynamics and Flow Technology, Spacecraft, 37073 Göttingen, Germany*

ABSTRACT

Flight tests have shown that the conditions in the base regions of space transportation systems are neither correctly predicted by CFD nor by experiments with cold exhaust jets. Experiments with a more realistic exhaust plume to study the temperature effects are required. In this study, a wind tunnel model concept is presented for representative plume interaction experiments in the *Vertical Test Section Cologne* (VMK) and the *Transonic Test Section Cologne* TMK. For this wind tunnel model, two combustion chambers are discussed. A thermal analysis is conducted for a *PennState*-like combustion chamber segment with a mixture ratio of 6.0 to evaluate the operating time in VMK. In order to cope with the conditions in TMK, the design of a second combustion chamber is designed to operate at a hydrogen-rich mixture ratio of 0.7. This involves the design and comparison of the inlet, stability and combustion chamber conditions for three different injector geometries. The study concludes with a proposition of materials for the combustion chamber.

Key words: hot plume interaction, jet, GH2/GO2 combustion chamber, exhaust gas, transonic wind tunnel tests, buffet/buffeting.

1. INTRODUCTION

During the ascent, space transportation systems are exposed to various hazardous conditions imposing high mechanical and thermal loads on the structure and components. The transonic flow regime has shown to be the most challenging. This is where the highest dynamic pressure occurs [1], buffeting poses a serious issue [2, 3], the ambient pressure has already decreased and promotes plume interaction [4, 5], mixing with the ambient flow leads to afterburning [4, 6] and radiation of the plume. The motivation for such base flow activities was elaborated in Ref. [7] and can be found in more detail in specialized literature like Ref. [8].

In the past, numerous investigations on this topic have been conducted. Experimentally, the exhaust plume was mostly represented either as a solid surface with the intention to simulate the corresponding displacement of the plume or as cold exhaust plume. Deprés et al. [3] showed that the pressure distribution and the spectral content on the base between a fluidic reattachment on a jet and a reattachment on the wall is comparable. In the frame of FESTIP program or with the FESTIP model, further experiments with respect to the interaction of the plume with the ambient flow were conducted [9, 10, 11]. The influence of an exhaust jet up to a stagnation temperature of $833\,\mathrm{K}$ was investigated by Zapryagaev et al. [12] and an increased base pressure due to the higher temperature was found in these experiments. This correlates with observations in flight where the base pressure is underestimated, thus the drag overestimated in comparison to cold plume experiments or CFD. For this reason, experiments with realistic hot exhaust jets just as planned with the upgrade of the *Vertical Test Section Cologne* [13, 14] to a hot plume interaction facility [7] at DLR Cologne are desirable.

Additionally, it is planned to upgrade the *Trisonic Test Section Cologne* (TMK) [15, 16] to equally facilitate hot plume interaction tests. Consequently, a suitable combustion chamber must be found for both facilities, whereas the limitations on the TMK wind tunnel model with the integrated combustion chamber are more restrictive with respect to size. The advantages of VMK are described in Ref. [7], which are essentially the possibility to facilitate an upstream supported and less size-restricted wind tunnel model, high safety standards due to the concrete walls, the verticality and open test section offers very good accessibility. TMK is advantageous since experiments can be conducted over a wider Mach number range. Further, TMK is equipped with a transonic measurement section with perforated walls for tests in the transonic flow regime. Since it does not feature an open test section, perturbations are avoided, which start at the wind tunnel nozzle exit due to an evolving shear layer as discussed in Ref. [17].

TMK, shown in Fig. 1, is a 'blow-down' type wind tunnel with a closed measurement section of $0.6 \times 0.6\,\mathrm{m}^2$ for tests in the trisonic flow regime ranging from sub-

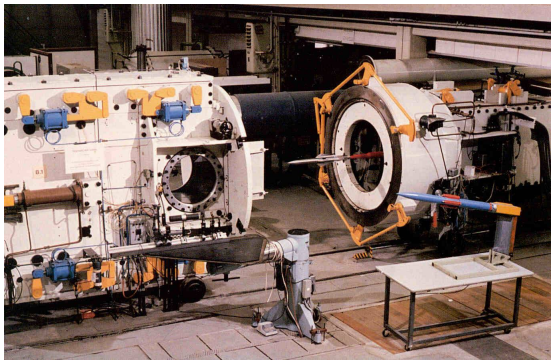

Figure 1. Image of Trisonic Test Section Cologne *(TMK).* [7]

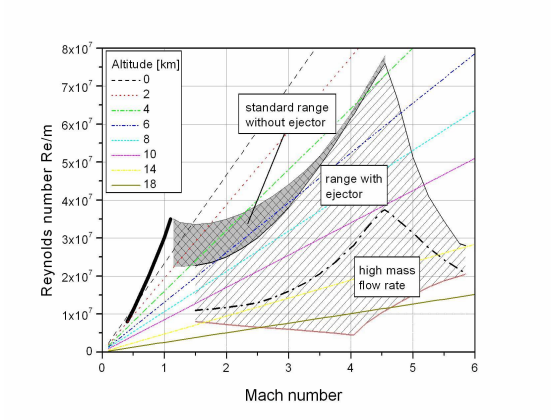

Figure 2. Operating range of Trisonic Test Section Cologne *(TMK).*

sonic Mach 0.5 to supersonic Mach 5.7. The Mach number can be adjusted continuously due to the flexible nozzle. The stagnation temperature can be set up to $550\,\mathrm{K}$ to avoid condensation or vary the Reynolds number. As shown in Fig. 2, an ejector permits to conduct tests over a wide Reynolds number regime even for high Mach numbers. Above Mach 4.5, the ejector is required to reduce the pressure downstream from the nozzle. In the past, TMK was mostly used for aerodynamic tests on missiles and spacecraft, the qualification of ramjet engine inlets, simulations of stage separation processes and propulsion jet simulation and side jet control experiments.

The wind tunnel model with the integrated *PennState*-like burner (Fig. 3), as considered for the VMK hot plume interaction facility [7], can not be implemented in TMK. This is shown in a thermal analysis in a first step based on a thermal analysis in Ch. 3. For the final state of a VMK upgrade, this *PennState*-like [18, 19, 20] combustion chamber made of oxygen-free high thermal conductivity (OFHC) copper is planned for experiments with realistically high mixture ratios. But, this combustion chamber and the inherent requirement for an appropri-

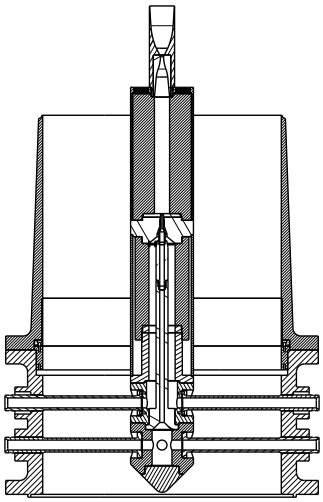

Figure 3. VMK wind tunnel model concept.

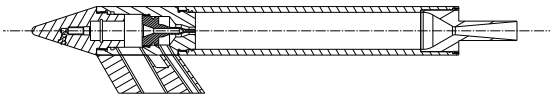

Figure 4. TMK wind tunnel model concept.

ately large wall thickness can not be integrated in a wind tunnel model and be accommodated in the TMK facility. Additionally, the operating time for a pressure higher than $2.07\,\mathrm{MPa}$ is very limited. Consequently, a wind tunnel model with a different combustion chamber is required for tests in TMK, which is shown in Fig. 4. To avoid unbearable loads on the materials of the wind tunnel model, a lower mixture ratio is chosen for the combustion chamber of the TMK wind tunnel model, which requires the determination of an appropriate injector. The design for such a hydrogen-rich chamber is presented as a second step. According to Ref. [21], the exhaust jet of such a chamber still features a high degree of similarity to flight. An exit velocity of up to 82% of the Vulcain engine can be reached. This velocity is approximated by an isentropic expansion in vacuum, while the mixture is treated as an ideal gas.

The inner combustion chamber geometry under investigation is shown in Fig. 5. It represents a modified version of the *PennState* burner [18] fitted for experiments in TMK [15, 16]. The changes concern the injector, the chamber length is shortened, the converging part toward the nozzle throat is less steep and the nozzle throat diameter is enlarged to $11\,\mathrm{mm}$. This increase is attributed to the baseline of the wind tunnel model, which is Ariane 5. Scaling considerations were conducted with the objective to define a nozzle with, on the one hand, a pressure ratio between the ambient and exit pressure

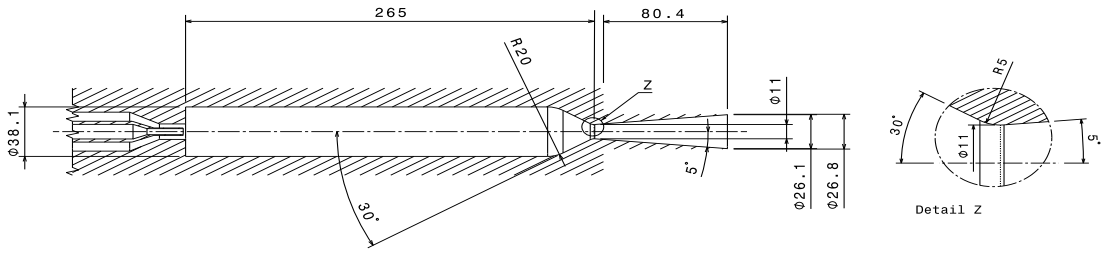

Figure 5. Inner geometry of the thrust chamber.

similar to the Ariane 5 flight in the transonic regime, and on the other hand, without exhibiting condensation of water in the exhaust plume for a mixing ratio of 0.7.
Both parameters are a function of the expansion ratio, which was set to approximately 5.6. This in turn leads to the exit diameter of the nozzle and, since similarity to Ariane 5 with respect to its main generic outer geometry was demanded (ratio between the diameter of the nozzle and the main body of 0.4), to the outer diameter of the main body of $67\,\mathrm{mm}$. With respect to the test section of TMK, this corresponds to a blockage ratio (without support) of 1% and, thus is suitable for testing in the transonic flow regime. The information about the exterior geometry is given as justification for the geometry and for completeness, but the study at hand focuses on the injector geometry and related properties in the combustion chamber.
Many investigations of the *PennState* burner yield to mixture ratios for high temperatures, meaning a hydrogen-rich injector for this chamber is not known to the authors and must be designed. The coaxial shear layer injector was chosen mostly due to its relevance, meaning the application in many rocket engines like Vulcain 2. Additionally, in a study by Calhoon et al. [22] where, among other aspects, different injectors were rated with respect to performance, compatibility, stability, insensitivity to engine variables, and design/fabricability, the coaxial shear layer element was ranked as one of the highest. Coaxial shear injectors feature a relatively low mixing rate in comparison to the triplet injector concept, but are advantageous concerning the fuel-rich, thus protective composition at the outer chamber wall.
The chamber geometry shown in Fig. 5 results in a characteristic chamber length of $L^\star = 3.3\,\mathrm{m}$ and features a stay time of $t^\star = 0.003\,\mathrm{s}$ for a chamber pressure of $2.07\,\mathrm{MPa}$, a mixture ratio of 0.7 and a throat diameter of $11\,\mathrm{mm}$. According to Sutton and Biblarz [8], typical characteristic lengths and stay times are between $0.8\,\mathrm{m}$ and $3.0\,\mathrm{m}$ and feature a stay time between $0.001\,\mathrm{s}$ and $0.040\,\mathrm{s}$ depending on the exact configuration or on the bipropellant in use. This comparison shows that the investigated chamber is rather on the large side with longer stay times, which supports one of the objective to facilitate a high combustion efficiency in the chamber. This in turn leads to a high degree of homogeneity at the exit of the nozzle for plume interaction investigations.

The objective of the paper at hand is to define a combustion chamber to facilitate hot plume interaction experiments in both wind tunnels, VMK and TMK. In a first step, a thermal analysis is conducted regarding the operating time of the *PennState*-like combustion chamber. A reduced heat load approach is then proposed and discussed. It simply implies the reduction of the mixture ratio to $O/F = 0.7$. In a last step, an injector geometry for the hydrogen-rich burner is designed and the results of such a combustion chamber are presented.

2. METHODS

The thermal analysis for the *PennState* burner was conducted with *ANSYS*. The outer wall is defined to be radiation-adiabatic. Potential cooling or heating by the wind tunnel flow is neglected. All other parameters are left on default values.

The *DLR Tau* [23, 24] code was used for the for the CFD simulations, which is a hybrid grid, finite volume second order accuracy flow solver. The simulations are based on Reynolds-averaged equation and the approach to calculate the combustion is equal to the investigations by Ivancic et al. [25]. The Menter SST eddy viscosity model with a Durbin realizability limitation [26]) is used. The reacting mixture is modeled as thermally perfect gas and the transportation equation is calculated for each individual species. The chemical source term in this set of transport equations is computed from the law of mass action by summation over all participating reactions. The modified Arrhenius law is applied for the forward reaction and the backward rate is determined from the equilibrium constant. The reaction mechanism is based on Gaffney's reduced 7-step, 6 species approach for hydrogen-air mixtures.
A sketch of one of the investigated injector geometries (config. 1) is given in Fig. 8. In total, three different configurations named as config. 1 to config. 3 are studied. The variation relates to the outer diameter of the annular passage (8.21, 9.4, $11.97\,\mathrm{mm}$) for hydrogen. An

Figure 6. Meshing of computational domain.

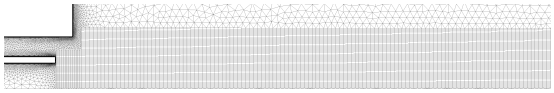

Figure 7. Mesh at the coaxial injector for config. 1.

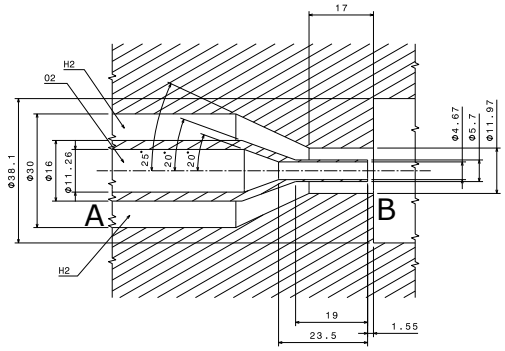

Figure 8. Geometry of the coaxial injector.

overview of the geometry and the input conditions (mass flow only) is given in Tab. 1.
The combustion chamber in the numerical simulation is approximated as being axisymmetric with adiabatic walls and supersonic outflow conditions. According to prior experiences, the computational domain (Fig. 6) is resolved with 180000 grid points and the wall-normal size of the wall-adjacent cell is $3 \cdot 10^{-6}$ m. More details of the mesh at the injector outlet can be seen in Fig. 7. The computational domain is discretized with a hybrid mesh with an increased number of cells in the assumed mixing region of the flame and a coarser resolution in the lateral direction. Only the mesh of one of the configurations (config. 2) is shown since the others are comparable in structure and resolution.

3. RESULTS & DISCUSSION

The thermal analysis is conducted with the objective to evaluate if a *PennState*-like burner is suitable for the application in TMK and VMK. One result of Ref. [18] is the heat flux profile in the axial direction along the wall for a mixture ratio of 6.0. This heat flux is imposed on a cylindrical segment of a combustion chamber made of copper for a chamber pressure of 2.07 MPa (300 psi) and 6.89 MPa (1000 psi). The results are shown for the

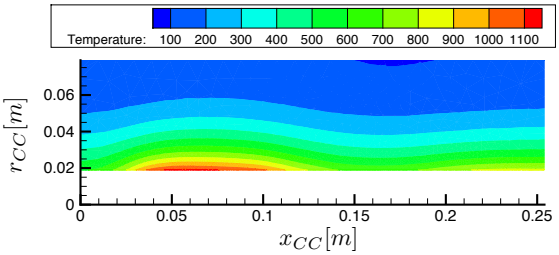

Figure 9. Temperature distribution of a copper thrust chamber after $t \approx 47.4$s for a heat flux rate corresponding to a chamber pressure of 2.07 MPa $=$ 300 psi.

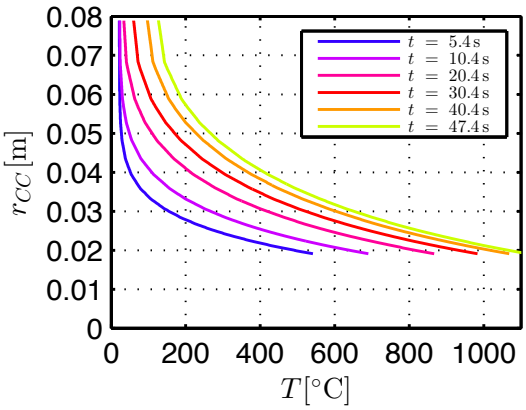

Figure 10. Temperature profiles at $x_{CC} = 51$ mm of a copper thrust chamber for a heat flux rate corresponding to a chamber pressure 2.07 MPa.

time step when the surface temperature of the combustion chamber exceeds 1080 °C, which is approximately the melting point of copper.

Fig. 9 depicts the temperature distribution for the 2.07 MPa case after 47.4 s. Obviously, the location where the highest temperature can be found corresponds to the location with highest heat flux given in Ref. [18]. The melting temperature is reached after 47.4 s, which is more than sufficient for testing in VMK with currently available measurement techniques. The transient behavior is depicted in Fig. 10 with the temperature profiles in radial direction of the thrust chamber for different times steps at the location with the highest heat flux (51 mm downstream from the injector). As expected, the wall absorbs and transports the heat towards the outer region. The energy transfer is fast enough to keep the surface wall temperature below the

Table 1. Boundary conditions for the simulation regarding the injector design.

Configuration			1	2	3
GOX mass flow	$\dot{m}_O$	gs^{-1}	36.7	36.7	36.7
GOX temperature	T_O	K	288.15	288.15	288.15
GH2 mass flow	$\dot{m}_F$	gs^{-1}	52.4	52.4	52.4
GH2 temperature	T_F	K	288.15	288.15	288.15
Throat diameter	d_{th}	mm	11.0	11.0	11.0
Mixture ratio	O/F	-	0.7	0.7	0.7
GOX central post inner diameter	d_{Ox}	mm	4.67	4.67	4.67
GH2 annular passage inner diameter	$d_{F,1}$	mm	5.7	5.7	5.7
GH2 annular passage outer diameter	$d_{F,2}$	mm	11.97	9.4	8.21
Recess	r	mm	1.55	1.55	1.55

melting point of copper for a sufficient testing time.

The $6.89\,\mathrm{MPa}$ case, which corresponds to the maximum pressure found for the *PennState* burner, is obviously exhibited to a more vigorous environment. The temperature distribution and temperature profiles in Fig. 11 and Fig. 12 reveal that the surface can only cope with that heat flux for about $2.6\,\mathrm{s}$ before the melting point of copper is reached. Heat transfer in the radial direction is not fast enough for a longer operating time. The considerations above show that a combustion chamber similar to the *PennState* burner require a large diameter to handle the heat loads, which can be realized with an upstream support in VMK as shown in Fig. 1 or discussed in Ref. [7]. VMK can run experiments with such a burner for about more than $40\,\mathrm{s}$, which is sufficient for most measurement techniques used in VMK. For longer runs, active cooling methods must be applied.

A different concept must be developed for transonic testing in TMK since the blockage ratio must be smaller than 1%, which can not be realized with the original *PennState* burner diameter. Based on similarity considerations, Frey [21] proposed a hydrogen-rich combustion chamber with a mixture ratio of 0.7, which can theoretically reach exit velocities in the range of the Vulcain 2 engine.

In this iterative design process, the injector designated with config. 1 is first investigated. It exhibits equal conditions at the outlet as the injector of the *PennState* burner [18] with respect to the outlet velocity ratio and momentum flux ratio. For the shortened combustion chamber, this results in an incomplete combustion, which can already be seen in the density profile in Fig. 13. The density at the outlet of the injector of config. 1 is lower compared to config. 2 and config. 3. As shown later, the oxygen is completely burned for the latter two configurations, which in turn leads to a higher combustion chamber temperature and pressure. The injectors of config. 2 and config. 3 must consequently be at the level of the combustion chamber pressure. The incomplete combustion is supported by the later discussed OH-concentration (Fig. 17). The level of the density profile adapts according to the combustion chamber pressure for the given temperature of $288.15\,\mathrm{K}$ at the inlet of the injector. Consequently, in order to increase the shear forces between the fluids, the annular passage for GH2 was decreased, which results in a higher outlet velocity as shown in Fig. 14. The last graph showing the Mach number (Fig. 15) reveals that none of the three configurations feature a choked injector outlet flow.

By means of the pressure drop over the injector and by comparing the results with Ref. [22], the stability of the combustion chamber is evaluated for config. 1 to 3. Tab. 2 lists the pressure upstream of the injector, the pressure in the combustion chamber and the corresponding pressure drop over the injector head, which is plotted in Fig. 16 along with the experimental findings of Calhoon et al. [22]. The letters A and B refer to the inlet and exit of the injector as shown in Fig. 8. The pressure drop of the oxidator line over the pressure drop of the fuel line can be seen and colors represent a stability assessment. The results of these experiments propose an unstable region for a pressure drop in the fuel line larger then approximately 0.1. According to this criteria, the coaxial injector config. 1 is stable, injector config. 2 is marginally stable and injector config. 3 is unstable. Despite the fact that this criteria seems not to be a strict limit and depends strongly on the specifics of the experiment, it is taken as an estimation for stability. Generally, it is stated in Ref. [22] that the lower mixture ratios tend to be more unstable. An increase in temperature (mixture ratio) or pressure has a stabilizing effect. But both aspects are counterproductive with respect to heat loads. Thus, the possible unstable behavior is accepted for the current state and an adaptation to the system might be necessary after the fabrication and testing.

The OH concentration in the combustion chamber for injector conf. 1 to 3 are shown Fig. 17 to Fig. 19, respectively. It can be seen that for injector conf. 1, the OH layer extends up to and through the nozzle throat indicating that the oxygen is not completely consumed in the combustion chamber. This finding is in accordance with the reduced density level at the injector outlet as shown in Fig.13. A decrease of the annular passage and the inherent increase of the fuel injector velocity decreases the stoichiometric mixing length significantly, which can be seen in Fig. 18 and Fig. 19 for injector config. 2 and con-

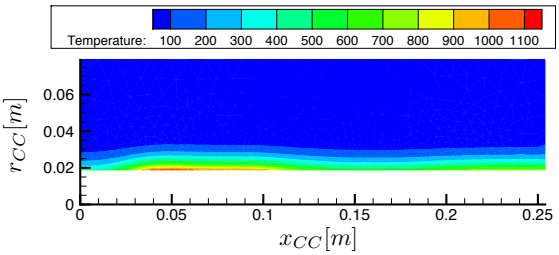

Figure 11. Temperature distribution of a copper thrust chamber after $t \approx 2.6\text{s}$ *for a heat flux rate corresponding to a chamber pressure of* $6.89\,\text{MPa} = 1000\,\text{psi}$.

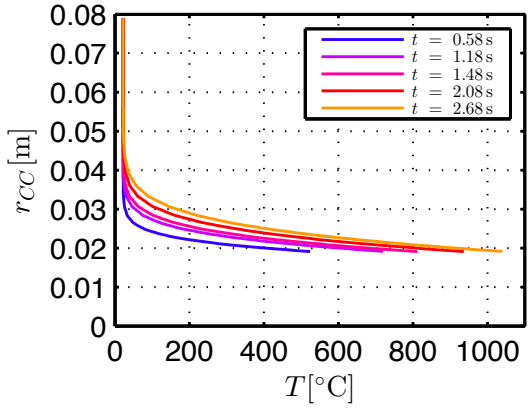

Figure 12. Temperature profiles at $x_{CC} = 51\,\text{mm}$ *of a copper thrust chamber for a heat flux rate corresponding to a chamber pressure* $6.89\,\text{MPa}$.

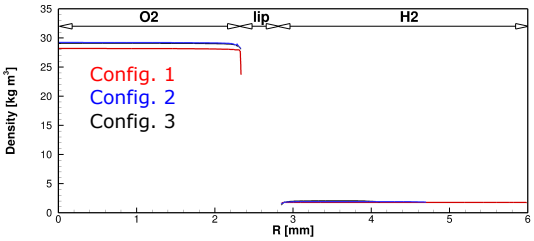

Figure 13. Density profile at the injector outlet.

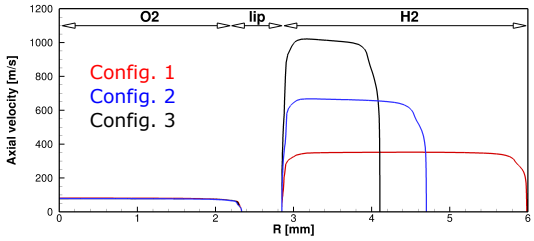

Figure 14. Axial velocity profile at the injector outlet.

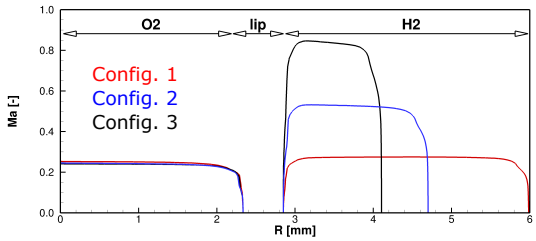

Figure 15. Mach number profile at the injector outlet.

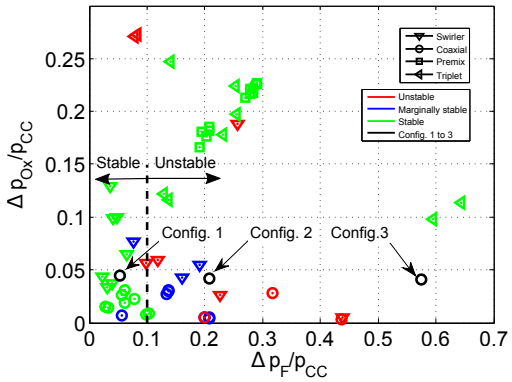

Figure 16. Low frequency stability characteristics of gaseous injector element Ref. [22].

fig. 3, respectively.

The mixing lengths L_S are depicted in Fig. 20 according to Schumaker and Driscoll [27] relation for the mixing length scaling along with the experiments from the corresponding study. It can be seen that config. 1 to config. 3 scale linearly as predicted by the scaling law given by $L_S/d_i = C_1(M^{0.5}X_S)^{-1}$. The mixing length is given by L_S, the inner diameter of the injector by d_i, C_1 is a scaling constant, X_S is the mole fraction of the inner jet fluid in a stoichiometric mixture and M represents the momentum flux ratio between hydrogen and oxygen. Just as for the experiments, a combustion chamber increase results in a steeper incline. The calculated mixing lengths for the higher pressure level in comparison to the experimental results seem plausible. The previous assessment showed that the species have not completely reacted in the combustion chamber for config. 1 and that config. 3 indicates an unstable combustion (Fig. 16). Consequently, the study is continued with the injector specified as config. 2. Fig. 21 to Fig. 23 show the Mach number with streamlines, the pressure and the temperature distribution inside the combustion chamber as contour plots, respectively. The Mach number contours show that only the Mach number is mainly elevated at the inlet to the combustion chamber, but decrease fast in the range of 0.1, meaning the flow is relatively slow and no compress-

Table 2. Conditions at coaxial injector inlet and outlet.

Configuration			1	2	3
Combustion chamber pressure	p_{CC}	MPa	2.090	2.169	2.166
GH2 injector inlet pressure (A)	$p_{F,i}$	MPa	2.189	2.592	3.349
GOX injector inlet pressure (A)	$p_{Ox,i}$	MPa	2.176	2.252	2.241
GH2 injector outlet pressure (B)	$p_{F,o}$	MPa	2.079	2.142	2.106
GOX injector outlet pressure (B)	$p_{Ox,o}$	MPa	2.083	2.161	2.153
GH2 injector outlet pressure (A/B)	$\Delta p_F/p_{CC}$	-	0.053	0.208	0.574
GOX injector pressure drop (A/B)	$\Delta p_{Ox}/p_{CC}$	-	0.045	0.042	0.41
GH2 injector outlet velocity (B)	$v_{F,o}$	ms^{-1}	352	664	1014
GOX injector outlet velocity (B)	$v_{Ox,o}$	ms^{-1}	80	78	78
GH2 injector outlet density (B)	$\rho_{F,o}$	kgm^{-3}	1.8	1.9	2.0
GOX injector outlet density (B)	$\rho_{Ox,o}$	kgm^{-3}	28.2	29.2	29.1
Injector outlet velocity ratio (B)	$v_{F,o}/v_{Ox,o}$	-	4.4	8.5	13.0
Injector outlet density ratio (B)	$\rho_{F,o}/\rho_{Ox,o}$	-	0.063	0.065	0.07
Injector momentum flux ratio (B)	$\rho_{F,o}v_{F,o}^2/(\rho_{Ox,o}v_{Ox,o}^2)$	-	1.27	4.7	11.8

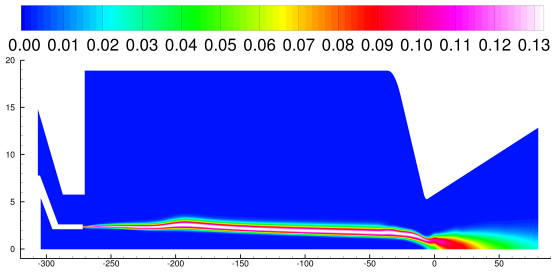

Figure 17. Contour plot of OH concentration in the combustion chamber for configuration 1.

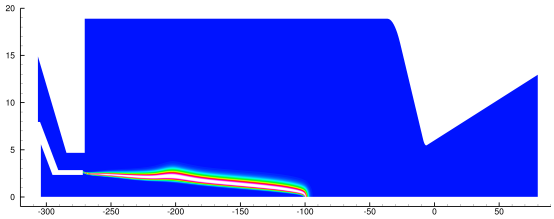

Figure 18. Contour plot of OH concentration in the combustion chamber for configuration 2.

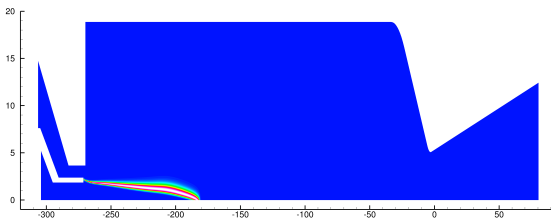

Figure 19. Contour plot of OH concentration in the combustion chamber for configuration 3.

ibility effects must be expected. The recirculation region depicted by the streamlines strongly resembles the results of comparable numerical simulations shown in Ref. [28] for a much higher mixture ratio. Fig. 22 shows the pressure drop over the injector head and a homogeneous pressure distribution in the combustion chamber since no acceleration is forced upon the flow due to geometry changes. The temperature distribution in Fig. 23 can be explained by the heat release of the flame. The reaction layer (Fig. 18) corresponds to the are the hottest region in the flow field. The mixing with hydrogen causes a cooler region in the lateral direction. Regions with cold gas can be found in the recirculation bubble fed by cold hydrogen gas and in the center where unburned oxygen is still present.

Temperature profiles along the combustion chamber for all three configurations are shown in Fig. 24. It shows that the highest temperature for adiabatic walls is reached just in the nozzle throat. There, injector config. 2 exhibits 860 K, which makes the application of high temperature-resistant steel possible. Ref. [29] gives a good overview to the materials used for gas generator-type combustion chambers. The materials in question for the combustion chamber can be *347 CRES, Hastelloy C, Haynes 25*,or an *Inconel* alloy. Since the temperature is rather low, the same material might also be applicable for the nozzle. Other options to be considered are nobium, pyrolitic graphite, tungsten or molybdenum.

4. CONCLUSION

The objective of this study was to define a suitable combination of wind tunnel model and combustion chamber to perform experiments for the investigation of the interaction phenomena between a representative exhaust jet of a rocket-like configuration and the exterior flow. It is planned to conduct experiments in the *Transonic Test*

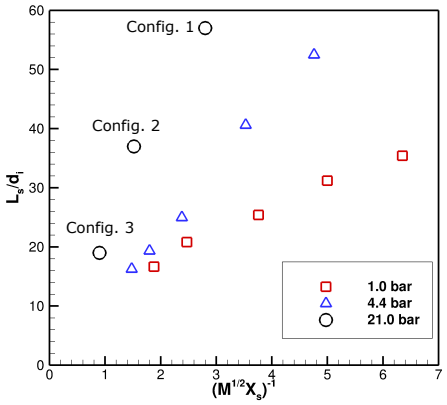

Figure 20. Effective momentum ratio scaling. The blue and red markers are extracted from experimental results by Schumaker and Driscoll [27]. The black markers correspond to the stoichiometric mixing given in Fig. 17 to 19.

Section Cologne (TMK) and in the *Vertical Test Section Cologne* (VMK). For interchangeable experiments, a combustion chamber is required for both. The thermal analysis showed that a *PennState*-like combustion chamber with a high mixture ratio can run for about 45 s at 2.07 MPa if large walls of OFHC are used. Due to size-restrictions, an integration of such a combustion chamber in a wind tunnel model is only acceptable for experiments in VMK. To meet the requirements for TMK, a hydrogen-rich combustion chamber was designed and numerically investigated. It was shown that the injector described as configuration 2 is most suitable since it ensures a stoichiometric mixing length within the combustion chamber. The results of the stoichiometric mixing lengths follow the scaling law by [27] and seem plausible. Attention must be paid to the stability of the combustion chamber. A comparison with [22] indicates a marginally stable behavior, meaning an adaptation to suppress pressure oscillations might be required. The temperature profile along the wall revealed that high temperature-resistant steel can handle the heat load of the hydrogen-rich combustion chamber, thus this combustion chamber can be integrated in a wind tunnel model for interaction experiments in TMK.

ACKNOWLEDGMENTS

This project is financially supported by the German Research Foundation (Deutsche Forschungsgemeinschaft – DFG) within the Transregional Collaborative Research Centre 40 (Sonderforschungsbereich Transregio 40). The help and advice of the technical staff of the *Supersonic and Hypersonic Technology Department* in Cologne is gratefully acknowledged.

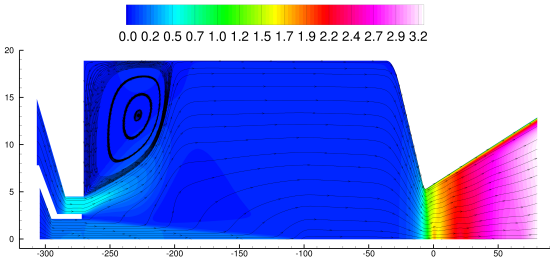

Figure 21. Contour plot of Mach number distrution in the combustion chamber for configuration 2.

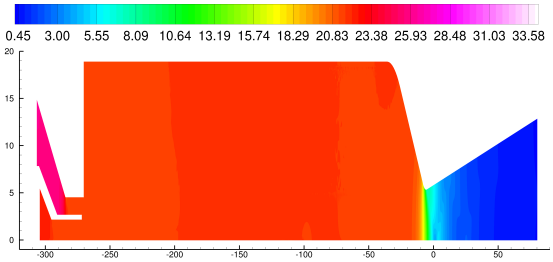

Figure 22. Contour plot pressure distribution in bar in the combustion chamber for configuration 2.

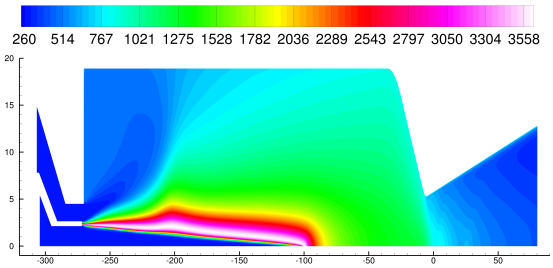

Figure 23. Contour plot of temperature distribution in Kelvin concentration in the combustion chamber for configuration 2.

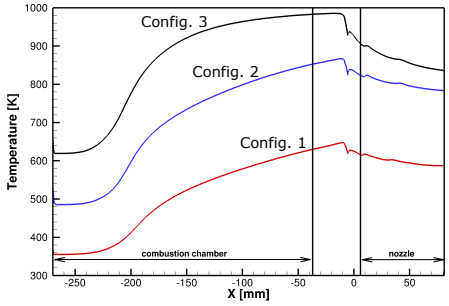

Figure 24. Wall temperature of the combustion chamber. Red, blue and black curve depict configuration 1, 2 and 3, respectively.

REFERENCES

[1] P. Leroux. Ariane 5 - Data relating to Flight 202. Launch kit, May 2011.

[2] S. Deck and P. Thorigny. Unsteadiness of an Axisymmetric Separating-Reattaching Flow: Numerical Investigation. *Physics of Fluids*, 19(6):065103, 2007.

[3] D. Deprés, P. Reijasse, and J.P. Dussauge. Analysis of Unsteadiness in Afterbody Transonic Flows. *AIAA journal*, 42(12):2541–2550, 2004.

[4] B.H. Goethert. Base Flow Characteristics of Missiles with Cluster-Rocket Exhausts. *Aerospace Engineering*, 20(3):28, 1961.

[5] H. Lüdeke and J.B. Calvo. A Fluid Structure Coupling of the Ariane-5 Nozzle Section during Start Phase by Detached Eddy Simulation. *CEAS Space Journal*, 1(1-4):33–44, 2011. ISSN 1868-2502. doi: 10.1007/s12567-010-0002-6. URL `http://dx.doi.org/10.1007/s12567-010-0002-6`.

[6] F.S. Simmons. *Rocket Exhaust Plume Phenomenology*. Aerospace Press El Segundo, CA, 2000.

[7] D. Saile and D. Kirchheck and A. Gülhan and D. Banuti. Design of a Hot Plume Interaction Facility at DLR Cologne. In *8th European Symposium on Aerothermodynamics for Space Vehicles*, 2015.

[8] G.P. Sutton and O. Biblarz. *Rocket Propulsion Rlements, 7th ed.* John Wiley & Sons, 2010.

[9] W.J. Bannink, P.O. Bakker, and E.M. Houtman. FESTIP Aerothermodynamics: Experimental Investigation of Base Flow and Exhaust Plume Interaction, Memorandum M-775. *Aerospace Engineering, Delft University of Technology*, 1997.

[10] M.M.J. Schoones and W.J. Bannink. Base Flow and Exhaust Plume Interaction. Part 1: Experimental Study. 1998.

[11] B.W. van Oudheusden and F. Scarano. PIV Investigation of Supersonic Base-Flow–Plume Interaction. In *Particle Image Velocimetry*, pages 465–474. Springer, 2008.

[12] V. Zapryagaev, A.V. Lokotko, S.V. Nikiforov, A.A. Pavlov, A.V. Tchernyshev, W.J. Bannink, H. Ottens, and J. Muylaert. Experimental Investigation of Base Pressure with Hot Supersonic Jet for External Supersonic Flow. In *Fourth Symposium on Aerothermodynamics for Space Vehicles*, volume 487, page 579, 2002.

[13] H. Esch. *Die 0,6x0,6-m-Trisonische Meßstrecke der DFVLR in Köln-Porz (Stand 1986), DFVLR-Mitt. 86-21*. Wissenschaftliches Berichtswesen der DFVLR, ISSN 0176-7739, Postfach 906058, 5000 Köln 90, 1986.

[14] Vertical Test Section Cologne (VMK), Supersonic and Hypersonic Technology Department. URL `http://www.dlr.de/as/en/desktopdefault.aspx/tabid-194/407_read-5445/`.

[15] K. Triesch and E.-O. Krohn. *Die Vertikale Meßstrecke der DFVLR in Köln-Porz (Stand 1986), DFVLR-Mitt. 86-22*. Wissenschaftliches Berichtswesen der DFVLR, ISSN 0176-7739, Postfach 906058, 5000 Köln 90, 1986.

[16] Trisonic Test Section Cologne (TMK), Supersonic and Hypersonic Technology Department. URL `http://www.dlr.de/as/en/desktopdefault.aspx/tabid-194/407_read-5447/`.

[17] P.E. Weiss and S. Deck. Numerical Investigation of the Robustness of an Axisymmetric Separating/Reattaching Flow to an External Perturbation Using ZDES. *Flow, turbulence and combustion*, 91 (3):697–715, 2013.

[18] W.M. Marshall, S. Pal, R.D. Woodward, and R.J. Santoro. Benchmark Wall Heat Flux Data for a GO2/GH2 Single Element Combustor. *AIAA Paper*, 3572:2005, 2005.

[19] P. Sibtosh, W. Marshall, R. Woodward, and R.J. Santoro. Test Case RCM-1: Penn State Preburner Combustor. In *3rd International Workshop Rocket Combustion Modeling, March 13-15, 2006, Vernon, France*, pages 1–9, 2006.

[20] P.K. Tucker, S. Menon, C.L. Merkler, J.C. Oefelein, and V. Yang. Validation of High-Fidelity CFD Simulations for Rocket Injector Design. *AIAA Paper*, 5226, 2008.

[21] M. Frey. TRP on Buffeting Reduction, WP3200: Feasibility Study for the Plume Simulation. *Doc. No. TP24-TN122/2009*, 1(1):19, 2009.

[22] D.F. Calhoon, J.I. Ito, and D.L. Kors. Investigation of Gaseous Propellant Combustion and Associated Injector/Chamber Design Guidelines. *NASA-CR-121234, N73 29799*, 1973.

[23] T. Gerhold, M. Galle, O. Friedrich, and J. Evans. Calculation of Complex Three Dimensional Configurations Employing the DLR-TAU-code. In *In Proceedings of the 35th Aerospace Sciences Meeting and Exhibit, number AIAA-1997-167, Reno, USA*, 1997.

[24] A. Mack and V. Hannemann. Validation of the Unstructured DLR-TAU-Code for Hypersonic Flows. In *In Proceedings of the 32nd AIAA Fluid Dynamics Conference and Exhibit, AIAA-2002-3111*, 2002.

[25] B. Ivancic, H. Riedmann, M. Frey, O. Knab, S. Karl, and K. Hannemann. Investigation of Different Modeling Approaches for CFD Simulation of High Pressure Rocket Combustors. In *EUCASS Book Series Advances in Aerospace Sciences: Progress in Propulsion Physics Volume 5*, 2015.

[26] P.A. Durbin. On the k-3 Stagnation Point Anomaly. *International Journal of Heat and Fluid Flow*, 17 (1):89–90, 1996.

[27] S. Schumaker and J. Driscoll. Mixing Lengths of Reacting and Nonreacting Coaxial Injectors in a Laboratory Rocket Combustor, AIAA 2008-5022.

44th AIAA/ASME/SAE/ASEE Joint Propulsion Conference & Exhibit, 21 - 23 July 2008, Hartford, CT, 2008.

[28] P.K. Tucker, S. Menon, C.L. Merkle, J.C. Oefelein, and V. Yang. Validation of High-Fidelity CFD Simulations for Rocket Injector Design. *AIAA Paper*, 5226:2008, 2008.

[29] H.W. Douglass, H.W. Schmidt, and L. Levinson. Liquid Propellant Gas Generators. *NASA SP-8081*, 1972.